ACS Sustainable Chemistry & Engineering

pubs.acs.org/journal/ascecg

Research Article

Mineral Manganese Oxides as Oxidation Catalysts: Capabilities in the CO-PROX Reaction

Arantxa Davó-Quiñonero,* Sergio López-Rodríguez, Esther Bailón-García, Dolores Lozano-Castelló, and Agustín Bueno-López

Cite This: *ACS Sustainable Chem. Eng.* 2021, 9, 6329−6336

Read Online

ACCESS | Metrics & More | Article Recommendations | Supporting Information

ABSTRACT: Cryptomelane is an abundant mineral manganese oxide with unique physicochemical features. This work investigates the real capabilities of cryptomelane as an oxidation catalyst. In particular, the preferential CO oxidation (CO-PROX), has been studied as a simple reaction model. When doped with copper, the cryptomelane-based material has revealed a great potential, displaying a comparable activity to the high-performance CuO/CeO_2. Despite stability concerns that compromise the primary catalyst reusability, CuO/cryptomelane is particularly robust in the presence of CO_2 and H_2O, typical components of realistic CO-PROX streams. The CO-PROX reaction mechanism has been assessed by means of isotopic oxygen pulse experiments. Altogether, CuO/CeO_2 shows a greater oxygen lability, which facilitates lattice oxygen enrolment in the CO-PROX mechanism. In the case of CuO/cryptomelane, in spite of its lower oxygen mobility, the intrinsic structural water co-assists as active oxygen species involved in CO-PROX. Thus, the presence of moisture in the reaction stream turns out to be beneficial for the stability of the cryptomelane structure, besides aiding into the active oxygen restitution in the catalyst. Overall, this study proves that CuO/cryptomelane is a promising competitor to CuO/CeO_2 in CO-PROX technology, whose implementation can bring the CO-PROX technology and H_2 purification processes a more sustainable nature.

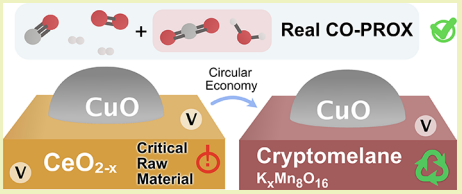

KEYWORDS: *rare earths, cryptomelane, cerium oxide, CO-PROX, reaction mechanism, isotopic oxygen, oxygen exchange*

INTRODUCTION

Rare-earth elements (REE), with manifold uses in civil, industrial, and military sectors as permanent magnets or housing and electronic components, are considered critical raw materials since potential disruptions in their supply would put our technology developments at risk.[1] Today, the REE market is rendered to a vulnerable chain supply by the dominance of China, which holds a powerful geostrategic position.[2,3] Besides, REE manufacture relies on polluting practices with dramatic environmental impact. Regretably, REE recycling technologies are not commercially implementable yet and merely supply 1% of the market.[4] Therefore, it is crucial to lower the REE demand by seeking functional substitute materials. This goal is a big scientific challenge owing to their unique magnetic, electrical, and optical properties, besides their well-recognized catalytic features.[5]

For instance, cerium oxides are renowned oxidation catalysts which have widely proven near-optimal catalytic performance several applications.[6] Among reliable catalytic alternatives to cerium oxide materials, manganese oxides are promising candidates. In contrast to REE minerals, mineral manganese oxides are abundant and their extraction and beneficiation can be achieved by means of non-toxic, inexpensive, and environmentally-friendly procedures.[7] In terms of catalytic activity, the mineral manganese oxide with the most promising catalytic properties is cryptomelane, which has attracted attention in the last years and centered some fundamental studies.[8−10] The versatility of cryptomelane-based materials is due to their high porosity, acidity, hydrophobicity, electronic and ionic conductivities, and easy removal of lattice oxygen and recovery. These features are provided by the facile redox cycling among Mn^{2+}, Mn^{3+}, and Mn^{4+} states, leading to an average manganese valence of *ca.* 3.8. Chemically, cryptomelane is a potassium−manganese mixed oxide consisting in a tunneled structure formed by double chains of corner-sharing MnO_6 octahedra basic units. The channel size left in between the 2 × 2 octahedra arrangement is 0.46 × 0.46 nm, and K ionic species and water molecules are hosted inside providing structural stability. The structure and composition of mineral cryptomelane can be achieved easily by inexpensive laboratory procedures leading to a synthetic material commonly named as octahedral molecular sieve 2 × 2 (OMS-2).[11]

In addition, it is well-known that the redox properties of cryptomelane can be tuned by means of the introduction of different framework dopants.[12−14] In particular, the best

Received: January 16, 2021
Revised: April 1, 2021
Published: April 26, 2021

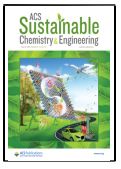

https://doi.org/10.1021/acssuschemeng.1c00343
ACS Sustainable Chem. Eng. 2021, 9, 6329−6336

catalytic improvements have been achieved with Cu^{2+} doping,[15,16] in an interesting analogy with the first CO oxidation hopcalite catalysts.[17] On the other hand, the interfacial redox properties occurring by means of synergistic effects in Cu-doped cryptomelane display similarities of the well-reported CuO/CeO_2 catalysts.[18] As a result of them, although Cu-modified cryptomelane materials are known to be more catalytically active systems than bare cryptomelane, Cu doping leads to a low thermal stability, which is a challenging limitation for their durable utilization in a hypothetic implemented use.

This work is aimed to provide a critical analysis of the feasibility of Cu-doped cryptomelane in terms of activity and stability to study its potential implementation and substitution of cerium oxides. Herein, a straightforward comparison between CuO/CeO_2 and CuO/cryptomelane catalytic systems is presented for the preferential CO oxidation reaction (CO-PROX) as the model case, which is relevant for the H_2-rich stream purification.[19] The catalytic performance and reusability under different gas mixtures has been tested, and the catalyst state after utilization has been carefully characterized. In addition, isotopic oxygen exchange experiments performed on the CuO/CeO_2 and CuO/cryptomelane systems have allowed to draw key mechanistic differences on the CO-PROX mechanism for the first time. In this study, the nature of the diverse active oxygen species existing in the ceria and the cryptomelane-based catalyst has been elucidated and their contributions in the CO oxidation mechanism evaluated. The results reveal promising opportunities for CuO/cryptomelane catalysts in the CO-PROX application, especially in the presence of moisture, because H_2O aids the regeneration of labile oxygen species in the cryptomelane structure. Thus, the implementation of cryptomelane-based catalysts is proven to be an efficient and more sustainable approach into the exhaustive catalytic CO clean-up required for H_2 safe use.

EXPERIMENTAL SECTION

Catalyst Synthesis. Two CuO/CeO_2 and CuO/cryptomelane catalysts were prepared with equivalent Cu nominal target on each metal oxide support. CeO_2 support was obtained via thermal decomposition of cerium(III) nitrate hexahydrate (Panreac) following a "flash" calcination at 500 °C in a preheated muffle furnace at 200 °C.[20,21] Synthetic cryptomelane was prepared following an adaptation from the so-called reflux method, procedure described by DeGuzman et al.[22,23] Particularly, 11 g of manganese(II) acetate (Aldrich) were dissolved in 40 g of water in a solution with a pH fixed at 5. After 30 min of reflux heating, potassium permanganate (Aldrich) solution (6.5 g/100 mL) was introduced and the boiling mixture was maintained with vigorous stirring for 24 h. The resulting dark-colored substance was filtered, washed until neutral pH, and dried at 120 °C overnight; its calcination at 450 °C for 2 h led to cryptomelane.

Once supports were prepared, the grinded powders were impregnated with an aqueous solution of $Cu(NO_3)_2{\cdot}(5{\cdot}1/2)H_2O$ (Panreac) to a target 5% nominal w. Cu content following the incipient wetness impregnation methodology. The impregnated samples were calcined to obtain CuO/CeO_2 and CuO/cryptomelane catalysts following the same heating protocol as the respective supports.

CO-PROX Activity Tests. The prepared materials were tested in CO-PROX catalytic activity experiments using a regular 100 mL/min flow of the gas reactant mixture (2% CO, 2% O_2, 30% H_2), set by means of Mass Flow Controllers (Bronkhorst). 150 mg of catalyst was placed in a quartz fixed-bed reactor (16 mm inner diameter, GHSV = ~30,000 h^{-1}) following a slow-pace heating ramp of 2 °C/min up to 200 °C. The reaction progress was monitored with a gas chromatograph HP model 6890 Plus Series coupled to a thermal conductivity detector. The effect of (1) CO_2, (2) H_2O and (3) CO_2 + H_2O in the catalytic activity was studied by means of the introduction of 9% CO_2, 5% H_2O, and 9% CO_2 + 5% H_2O, respectively, in the reactant gas mixture feeding.

Catalyst Characterization. N_2 adsorption−desorption isotherms were performed in an automatic volumetric system (Autosorb-6, Quantachrome) after outgassing the samples at 150 °C for 4 h (Figure S1, Table S1). Transmission electron microscopy (TEM) characterization was conducted using a JEOL (JEM-2010) microscope (Figure S2). Fresh and spent samples were characterized by means of X-ray diffraction (XRD) for the crystalline resolution using a Bruker D8-ADVANCE diffractometer using Cu Kα radiation. Diffractograms were recorded at 2θ between 10 and 90°, with a step size of 0.05° and a time of 3 s per step.

Temperature-programmed reduction experiments with H_2 (H_2-TPR) were conducted in a Micromeritics Pulse Chemisorb 2705 instrument. 40 mg of the catalyst was placed in a quartz tubular reactor under 40 mL/min of 5% H_2/Ar gas mixture following a heating ramp of 10 °C/min.

Temperature-programmed desorption (TPD) experiments were conducted with 80 mg of the catalyst after a pre-treatment at 400 °C for 30 min in a 100 mL/min flow of Ar. Then, a saturation step with the selected gases was carried out, which consisted of heating the catalyst at 150 °C for 1 h under 100 mL/min of 10% CO_2/Ar (for CO_2-TPD), 5% H_2O/Ar (for H_2O-TPD), or 10% CO_2 + 5% H_2O/Ar (for CO_2 + H_2O-TPD). After that, the gas mixture was switched to Ar, and once CO_2 and H_2O signals were stabilized, the reactor was heated from 150 to 650 °C following a ramp of 10 °C/min in 100 mL/min of Ar.

Isotopic $^{36}O_2$ Pulse Experiments. Isotopic exchange experiments were carried out with $^{36}O_2$ by means of an injection valve with a loop (100 μL) and two high sensitivity pressure transducers. The experiments were carried out in a fixed-bed tubular quartz reactor with 80 mg of catalyst in a constant 20 mL/min of 1% CO, 30% H_2-balanced He feeding mixture. The exhaust gases were monitored with MS, and the $^{36}O_2$ pulses (Isotec, 99%; 100 μL and 9 psi) were injected at 75, 100, and 150 °C once achieving signal stabilization. Prior to this, several pulses of Ar (100 μL and 9 psi) were used as a test to confirm reproducibility of the method.

RESULTS

CO-PROX Activity Tests. Figure 1a,b shows the temperature for the 50% of CO conversion (T_{50}) along four consecutive CO-PROX catalytic runs, which allows us to evaluate the stability and recyclability of CuO/CeO_2 and CuO/cryptomelane catalysts. The CO-PROX light-off curves are compiled in Figure S3a,b,c,d, respectively. As shown, both catalysts reach CO conversion (and CuO/Cryptomelane catalysts are compiled in Figure S3a,b and Figure S3c,d, respectively). As shown, both catalysts reach CO conversion (X_{CO}) values of 94−98% in the low temperature window of CO-PROX regardless the conditions, besides CO selectivity (*Sel.*) is maintained close to the optimum (50% according to the feeding O_2/CO stoichiometry).

The inhibiting effect of the CO_2, H_2O, and CO_2 + H_2O mixture in the reactor feeding stream follows the trend CO_2 < H_2O < CO_2 + H_2O for both catalysts, in agreement with the reported literature.[15,24−26] Interestingly, the impact of H_2O in the CO oxidation catalytic activity results more detrimental than CO_2 itself. In CuO/CeO_2, the interaction with CO_2 leads to an intense carbonatation besides the formation of stable formates, carboxylates, and bicarbonates, which hamper Cu−Ce interaction and inhibit CO oxidation.[24,25] On the contrary, the CO-PROX catalytic activity of CuO/cryptomelane is fairly not affected by CO_2, but it is very sensitive to H_2O. On the other hand, CO_2 + H_2O conditions lead to the strongest

https://doi.org/10.1021/acssuschemeng.1c00343
ACS Sustainable Chem. Eng. 2021, 9, 6329−6336

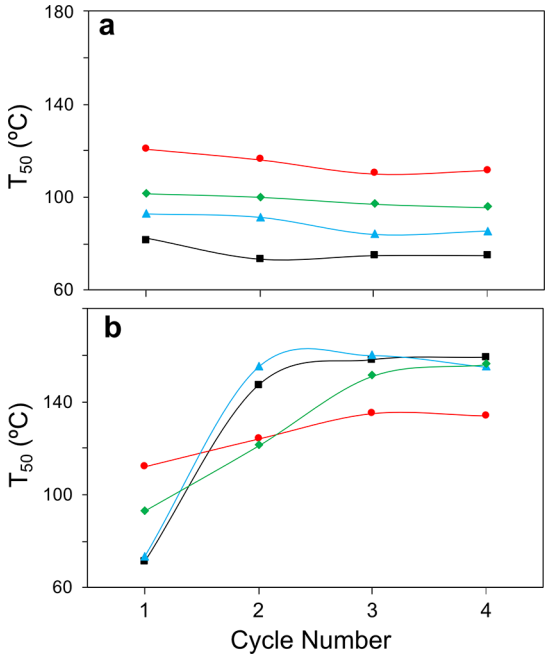

Figure 1. Temperature for the 50% of CO conversion (T_{50}) in 1−4 cycles of CO-PROX reaction in different environment mixtures: CO + O_2 + H_2 (squares), CO + O_2 + H_2 + CO_2 (triangles), CO + O_2 + H_2 + H_2O (diamonds), CO + O_2 + H_2 + CO_2 + H_2O (circles) for (a) CuO/CeO_2; (b) CuO/cryptomelane catalysts.

inhibition state, suggesting the participation of both species in co-adsorptive processes.[15,27]

According to Figure 1, CuO/CeO_2 presents a stable behavior within four cycles of reaction in all the tested conditions, while CuO/cryptomelane suffers from a deactivating process of different magnitude as seen by the T_{50} increase alongside the number of reaction runs. This degradation is spurred by ongoing oxidation−reduction cycles during CO-PROX that lead to the inactive Mn_3O_4,[8,28] which was proven to be partially reversible by means of oxidative regeneration treatments.[29]

Comparing both catalysts, CuO/cryptomelane presents an enhanced catalytic activity with regard to CuO/CeO_2 in a first run for all the set of conditions. However, the deactivation of CuO/cryptomelane leads to the opposite trend beyond the second cycle. CO_2 + H_2O conditions confer the greatest stability to CuO/cryptomelane and in result, the best performance in the fourth cycle. In this atmosphere, CuO/cryptomelane displays an admirable activity as compared with CuO/CeO_2 (T_{50} of 134 and 117 °C, respectively). Because CO-PROX reaction under CO_2 and H_2O presence is the most challenging, but also the most representative of the realistic operation, the promising potential of CuO/cryptomelane deserves to be further investigated.

Understanding the Catalyst Stability under CO_2 and H_2O Mixtures. As typical for Mn^{4+}-based minerals, cryptomelane is dark-colored and operando infrared spectroscopy measures fail due to its high absorption, showing blackout IR spectra. Therefore, the study of the reaction mechanism must be assessed by alternative and complementary techniques.

The Supporting Information document contains the characterization results of fresh and spent catalyst samples in the different conditions tested. Namely, XRD (Figure S4a,b, Tables S2 and S3) and H_2-TPR (Figure S5a,b) which confirm that CuO/CeO_2 catalyst presents a robust crystalline structure, whereas CuO/cryptomelane displays a poor stability under CO-PROX reaction in CO + O_2 + H_2 conditions, after which, Mn_3O_4 (hausmannite) is the main crystalline phase. The transition from cryptomelane ($K_xMn_8O_{16}$) to Mn_3O_4 involves the collapse of the characteristic 2 × 2 tunnels of cryptomelane besides the reduction of Mn cations from an average oxidation state of *ca.* +3.8 to +2.5. The degradation of the cryptomelane microstructure occurs when the intratunnel K is segregated to the outer surface and probably released in the form of K volatile species.[30,31] The loss of charge-compensating K species leads to the reduction of the manganese ions left upon cryptomelane collapse.[32,33] Figure S2e,f shows TEM images of the deactivated CuO/cryptomelane catalyst, displaying non-aggregated Mn oxide particles around the deteriorated nanorod array. In our previous work,[29] we studied the CuO/cryptomelane deactivated material left upon CO-PROX cycles, and no significant textural differences compared to the fresh sample related to this transition phase were found. However, we reported evidences of potassium segregation, manganese reduction, and the formation of copper species with high charge density. The presence of these partially reduced copper species with the atypical XPS binding energy of *ca.* 930.5 eV is well reported for the hopcalite $CuMn_2O_4$ spent and deactivated material, which suffers an amorphous to crystalline transition.[34,35] In the case of deactivated CuO/cryptomelane samples, Cu^{n+} species at that low binding energy are ascribed to Cu^+ being located in an octahedral site in the spinel structure, subjected to a larger extra-atomic relaxation energy.[17,36] Finally, as in the case of the CuO/CeO_2 catalyst, tenorite peaks from the segregated CuO phase is not detectable in the X-ray diffractograms of CuO/cryptomelane (see Figure S4a,b). The absence of CuO peaks reveals that the copper phase is well dispersed before and after the reaction runs. On the other hand, the co-addition of CO_2 + H_2O in the CO-PROX gas reactant mixture leads to the preservation of the cryptomelane structure (see Table S3).

Regarding the redox features, H_2-TPR profiles (Figure S5a,b) reveal that CuO/CeO_2 samples experience changes in Cu−Ce interaction after the CO-PROX reaction cycles, which are hints of CuO sintering or Cu−Ce contact modification.[37,38] However, these do not reflect into any sort of activity loss. For CuO/cryptomelane, H_2-TPR profiles exhibit large differences depending on the catalyst state. Nevertheless, the spent sample in CO_2 + H_2O conditions shows discrepancies with the fresh sample; the manganese reduction events roughly keep the shape and position in the profile. For the sample used in the experiments free of CO_2 + H_2O, the reduction profile presents a very different aspect, which can be attributed to the cryptomelane phase distortion and reduction toward the hausmannite phase.

TPD experiments (Figure 2a−f) for CuO/CeO_2 and CuO/cryptomelane after CO_2, H_2O, and CO_2 + H_2O exposures provide relevant insights about the catalyst interaction with CO_2 and H_2O. As depicted, CeO_2 has a great capacity to stabilize carbonaceous species on surface due to its high basicity. On the contrary, cryptomelane has very moderate affinity for CO_2, in agreement with the low impact of CO_2 addition in the CO-PROX activity tests. In both cases, H_2O is co-released, which can be attributed to the depletion of the inherently present hydroxyls upon carbonate and bicarbonate decomposition. Analogously, after H_2O saturation, H_2O and

https://doi.org/10.1021/acssuschemeng.1c00343
ACS Sustainable Chem. Eng. 2021, 9, 6329−6336

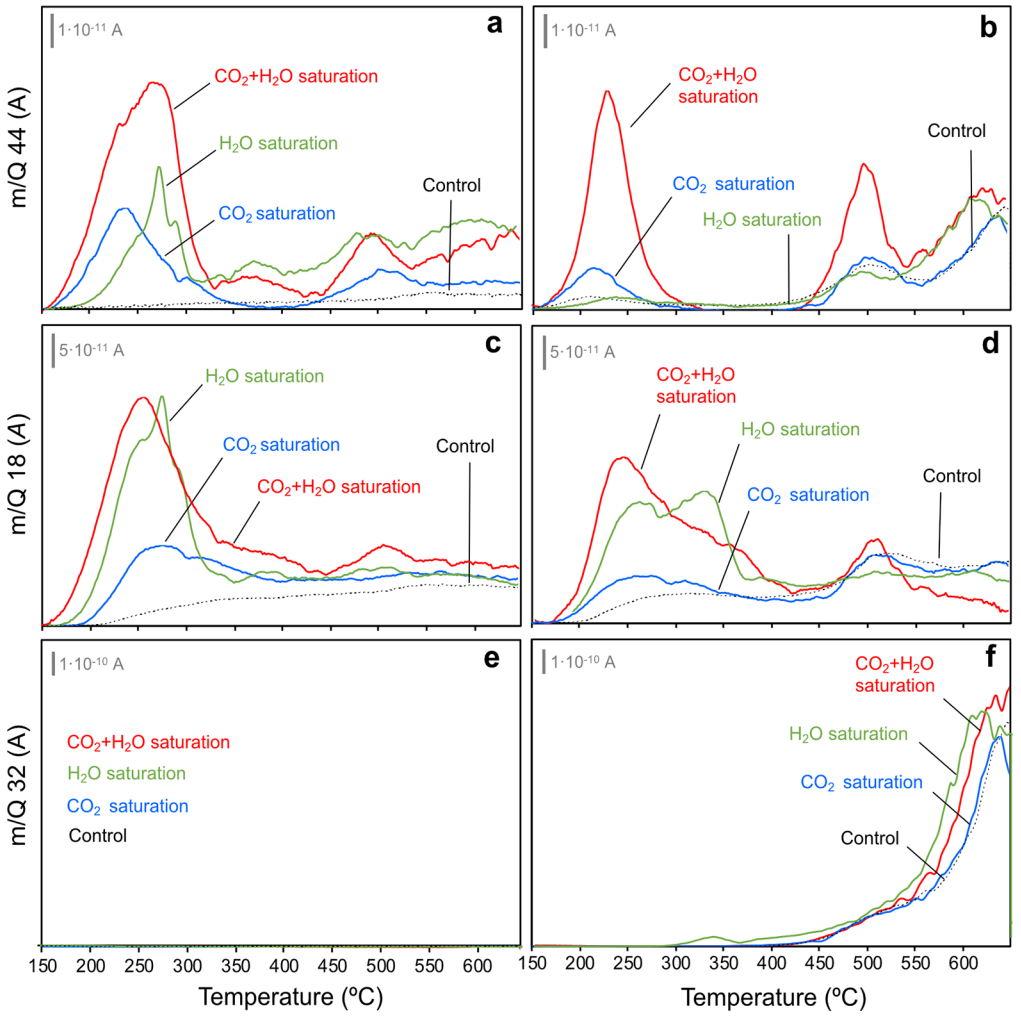

Figure 2. Monitored MS signals (a,b) 44, CO_2; (c,d) 18, H_2O; and (e,f) 32, O_2 for (a,c,e) CuO/CeO_2; and (b,d,f) CuO/cryptomelane catalysts in CO_2-TPD; H_2O-TPD; and (CO_2 + H_2O)-TPD experiments.

CO_2 co-evolve and CO_2−H_2O interaction is maximized, as CuO/CeO_2 exhibits in these conditions a larger CO_2 release than after CO_2 saturation itself.[39] Thus, H_2O in contact to CuO/CeO_2 catalyst may favor the release of intrinsically present stable carbonates.

In the case of CuO/cryptomelane, the CO_2−H_2O co-release upon the individual gas exposure is not so relevant, and on the other hand, cryptomelane is much more prone to interact with H_2O than with CO_2. However, the concomitant addition of CO_2 + H_2O leads to a sharp growth of CO_2 and H_2O release, which is indicative of a favored CO_2−H_2O co-adsorption as in the case of CuO/CeO_2. For CuO/cryptomelane, since it shows a low affinity toward bare CO_2 chemisorption, CO_2 is inferred to be retained as hydrogenated carbon intermediates, such as bicarbonates on the cryptomelane acidic surface.

Finally, the O_2 profile (MS signal of 32, Figure 2e) shows that CuO/CeO_2 is thermally stable since it presents a negligible flat product release up to the maximum temperature of the experiment (*i.e.*, 650 °C). In contrast, CuO/cryptomelane displays a significant O_2 release (Figure 2f) which starts decomposing above 450 °C. Remarkably, the CuO/cryptomelane decomposition occurs equally regardless the nature of the saturation treatment, which differs from the enhanced stability assessed for CuO/cryptomelane in the CO_2 + H_2O CO-PROX tests. Thus, the positive effect of CO_2 + H_2O on cryptomelane during the CO-PROX reaction cannot be merely superficial, and other factors must be at play involving the catalyst oxidation−reduction cyclability.

Isotopic $^{36}O_2$ Pulse Experiments. Pulse oxygen isotopic experiments in CO-PROX conditions at selected temperatures were conducted for both CuO/CeO_2 and CuO/cryptomelane samples (Figure 3a−f). For the critical comparison between both catalysts, the monitored MS signals were normalized in terms of total O species (CO_2 + H_2O + O_2). The time evolution of the pulses at different temperatures is depicted in Figure 3a−f, while the quantification of the released products is presented in Figure 4a,b. Noticeably, in the CuO/CeO_2 catalyst, no trace of O_2 signals was found at any of the tested temperatures after the $^{36}O_2$ pulse. This indicates that the catalyst fully uptakes the incoming O_2, accommodating oxygen into the lattice as the anionic vacancies created upon the reducing conditions of the experiment are refilled. This labile restorage after the isotopic oxygen pulse leads to the destabilization of the adsorbed CO and H_2 molecules, being released as and their oxidation products (*i.e.*, CO_2 and H_2O). The analysis of the product distribution evolved reveals that CO and H_2 oxidation reactions occur mainly involving lattice oxygen (^{16}O), as well reported for CuO/CeO_2 catalysts displaying a Mars−van Krevelen (MVK).[40−42] In this regard, the temperature does not affect significantly the isotopic

https://doi.org/10.1021/acssuschemeng.1c00343
ACS Sustainable Chem. Eng. 2021, 9, 6329−6336

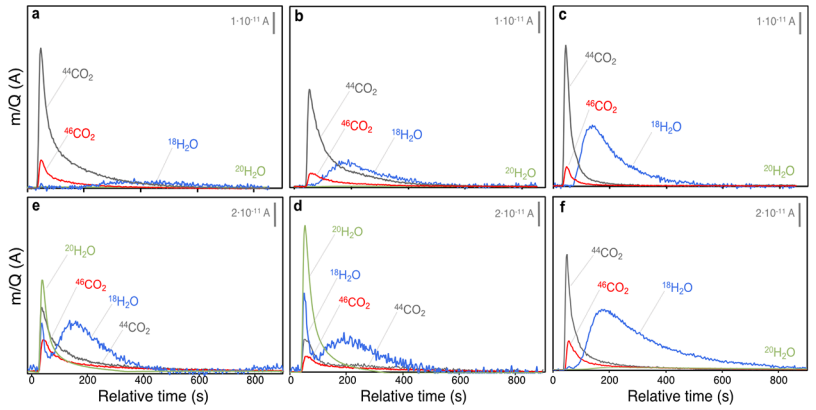

Figure 3. MS signals after $^{36}O_2$ pulses in CO-PROX conditions with (a–c) CuO/CeO_2 and (d–f) CuO/cryptomelane catalyst at (a,d) 75, (b,e) 100, and (c,f) 150 °C. Zero-time refers to the pulse injection in the reactor.

product share within the 75–150 °C range, but it does to the global yield to CO_2 and H_2O, in good correlation with the selectivity fall observed in fixed-bed catalytic. Thus, $^{20}H_2O$ is not detected, whereas the release of $^{18}H_2O$ is delayed in time compared to CO_2-type products. This decoupling of the CO_2 and H_2O evolution can be attributed to greater desorption limitations of H_2O on the surface of CeO_2.

For the CuO/cryptomelane catalyst, Figure 3d–f shows the evolved products after the $^{36}O_2$ pulses at the different temperatures, and significant differences are found when compared to CuO/CeO_2. First, the release of a large amount of H_2O at low temperatures disrupts the well-correlated CO selectivity profiles of pulse experiments to fix-bed catalytic tests as in the CuO/CeO_2 catalyst. Furthermore, the distribution of CO_2 and H_2O products is a mixture between isotopic and non-isotopic, rather than clearly non-isotopic as for CuO/CeO_2, which indicates a poorer oxygen exchange capacity for CuO/cryptomelane. In order to evaluate this, Figure 4a,b shows for both catalysts the integrated signals for the released products from H_2O and CO_2 formation upon H_2 and CO oxidation after the pulse (solid symbols), as well as the overall outlet H_2O, CO_2, and O_2 measured (open symbols).

As depicted, CO_2 and H_2O profiles are more complex in the case of CuO/cryptomelane and the effect of temperature is more relevant in the distribution of the evolved species. In this case, upon interaction with the CuO/cryptomelane surface, most of the incoming isotopic $^{36}O_2$ molecules leads to $^{20}H_2O$, which is released after the pulse with no apparent desorption limitations. On the other hand, the oxygen pulse destabilizes the intrinsically present H_2O molecules, resulting in a large $^{18}H_2O$ (non-isotopic) co-emission. In contrast with $^{20}H_2O$, two different contributions of $^{18}H_2O$ are discerned, being one anticipated and released at the same time of $^{20}H_2O$ and CO_2 species, and the other retarded as H_2O in the CuO/CeO_2 catalyst. According to the H_2O desorption profile (Figure 2e), CuO/cryptomelane would release two types of H_2O in the low-temperature region, attributed to surface-related water and water bounded inside the 2 × 2 tunnels. Hence, the first H_2O contribution must be tentatively assigned to the mobilization of the intrinsic intratunnel water molecules that undergo a labile exchange with the incoming $^{36}O_2$ molecules, resulting in a sharp co-emission of $^{18}H_2O$ and $^{20}H_2O$. As it has been discussed elsewhere,[31,33] the activity of the CuO/cryptomelane catalyst is related to the presence of highly mobile water species hosted in the tunnels, which provide good ionic

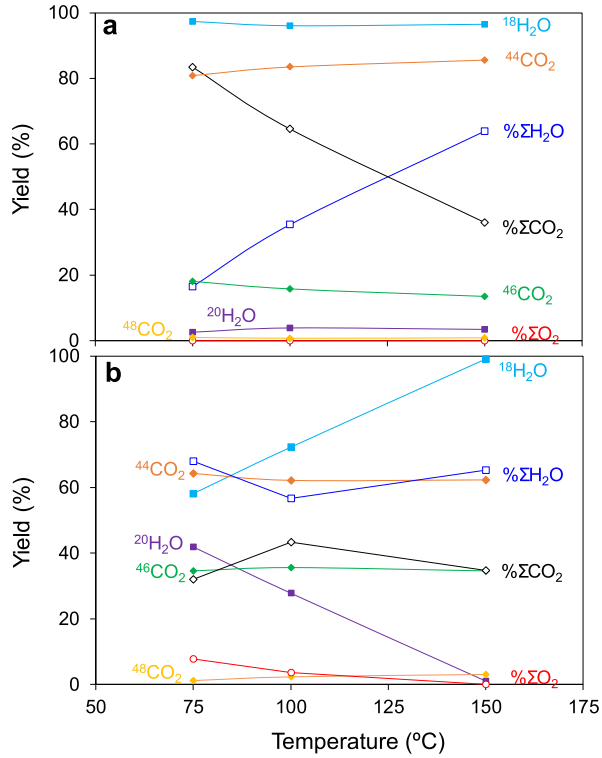

Figure 4. MS-normalized signals after $^{36}O_2$ pulses in CO-PROX conditions with (a) CuO/CeO_2, (b) CuO/cryptomelane catalyst at 75, 100, and 150 °C. (Solid symbols): overall O_2 released species in the outlet flow; (open symbols): isotopic distribution among H_2O and CO_2 species.

mobility and stabilize the cryptomelane framework. Thus, the CuO/cryptomelane crystalline nature and catalytic activity features rely on such bounded H_2O molecules, as partial O exchange in water is indeed observed. The temperature has an effect in lowering the evolution of the anticipated H_2O, which is in agreement with the cryptomelane collapse toward the formation of the average reduced Mn_3O_4 spinel phase, as a result of the massive water loss caused by the CO-PROX reaction conditions. So that, at high temperatures in the CO + H_2 conditions of the pulse experiments, the CuO/cryptomelane catalyst is gradually reduced and consequently, the amount of released water decreases, until at 150 °C, cryptomelane is in overall reduced. In such state, intra-tunnel

https://doi.org/10.1021/acssuschemeng.1c00343
ACS Sustainable Chem. Eng. 2021, 9, 6329–6336

water species are not found to be released either because they are totally depleted or because the remaining species is so tightly bounded that are not mobilized after the pulse. Thus, only beyond 150 °C, the outlet water comes solely from H_2 oxidation reaction, and the release of such delayed H_2O evidently has a more relevant contribution in the overall CO_2 + H_2O distribution than in the equivalent conditions for CuO/CeO_2. This apparent lower CO selectivity of CuO/cryptomelane needs to be rationalized, given the large affinity of CuO/cryptomelane to water and the strong driving force found that releases intratunnel hosted species in the conditions of the experiment. On the contrary, the isotopic CO_2 components are free of this masking effect from cryptomelane intrinsic water. Thus, compared to CuO/CeO_2, CuO/cryptomelane exhibits a lowered contribution for the non-isotopic $^{44}CO_2$ species, that is, lesser participation in the MVK mechanism due to a less active lattice oxygen species. As a result, whereas CuO/CeO_2 efficiently uptakes the pulsed O_2 molecules in the anionic lattice vacancies, CuO/cryptomelane exchanges O from structural water, which is partially released as isotopic $^{20}H_2O$ without accommodating the integrity of the O_2 pulse. In this case, the O restorage from the pulse is high, but not complete at 75 and 100 °C (see Figure S6) since the O-catalyst preferential interaction occurs within the intratunnel water molecules rather than through direct O-lattice restoration in the MnO_6 octahedra framework. Finally, at 150 °C, the system reaches the non-selective regime, where producing H_2O is released as the major reaction product. Onwards, H_2O products are majority regardless of the temperature.

GENERAL DISCUSSION

The relative participation of lattice oxygen in the CO oxidation (MVK) mechanism of reaction is greater in the CuO/CeO_2 catalyst than in the CuO/cryptomelane, evidenced by the larger emission of non-isotopic products after the pulses. In contact with CuO/cryptomelane, incoming O_2 molecules preferentially interact with the labile H_2O species hosted in the tunnels, which are a key element of cryptomelane good oxidation activity. These species turn into quick oxygen exchange sites and mediate into the oxygen restoration, besides preventing extensive H_2O release toward cryptomelane collapse. When H_2O is supplied in the CO-PROX reactor, CuO/cryptomelane maintains a better performance along catalytic cycles, given its faster reoxidation capacity mediated via H_2O. The positive complementary effect of CO_2 cannot be ruled out since the best performance at the fourth cycle occurs in CO_2 + H_2O conditions, as shown in Figure 1b. A possible explanation is the maximization of the H_2O retention capacity by the maximization of H_2O interaction with the cryptomelane surface promoted when H_2O and CO_2 are co-supplied, in agreement with TPD results. TPD profiles also show that CO_2 + H_2O saturation incentivizes the low-temperature water desorption (150−300 °C), attributed to surface water, in detriment of the higher temperature contribution (300−375 °C), attributed to intratunnel water. Hence, CO_2 presence aids to stabilize intratunnel water, preventing its release after CO_2 + H_2O contact when compared to lone H_2O. Cryptomelane stability is improved. The characteristic redox features are better maintained with the co-addition of CO_2, as well as CO_2 retention is enlarged in the stabilization of hydrogen-carbonated intermediates. In turn, the surface coverage of labile carbonaceous intermediates with a facile desorption protects the O-lattice abstraction and cryptomelane reduction upon CO and H_2 oxidation reactions, resulting in a hindered activity, but eventually a greater stability.

CONCLUSIONS

The CO-PROX catalytic performance and reaction mechanism have been addressed in CuO/CeO_2 and CuO/cryptomelane catalysts. In the first run, the catalytic activities of CuO/CeO_2 and CuO/cryptomelane are comparable, being both excellent materials for this application even in real operation conditions, including CO_2 + H_2O in the feeding stream. In CuO/CeO_2, both CO_2 and H_2O are inhibited by surface blockage, where H_2O has more impact. On the contrary, CuO/cryptomelane is not affected by CO_2 presence but strongly inhibited by H_2O. In terms of cyclability and reusability, CuO/CeO_2 maintains the activity along, at least, four catalytic cycles regardless of the ambient conditions. However, CuO/cryptomelane suffers from severe deactivation related to structural collapse and partial reduction from cryptomelane phase (MnO_2) to hausmannite (Mn_3O_4), and the extent of such deactivation depends on the inlet gas mixture. Namely, CO_2 + H_2O conditions prevent CuO/cryptomelane decomposition, enabling to achieve the best catalytic performance at the fourth cycle, conditions where the near-optimal CuO/CeO_2 catalyst exhibits its worst catalytic behavior.

In conclusion, CuO/cryptomelane demonstrates to be a potential competitor to CuO/CeO_2 in CO-PROX technologies under realistic operation conditions. This outcome opens up an era of possibilities toward a sustainable non-REE based catalysis yet to scale and test in the future. Up to now, green and efficient catalysts based on active copper−manganese formulation designed in this study are proven to be sufficiently good candidates, once established the best reaction protocols. Future studies will allow improvement on the stability in long term and cyclic operations of cryptomelane-based systems, as well as to broaden the battery of active materials of similar nature. This knowledge can be extended to analogue studies of other minerals toward the design of the optimum Cu−Mn catalytic synergism.

ASSOCIATED CONTENT

Supporting Information

The Supporting Information is available free of charge at https://pubs.acs.org/doi/10.1021/acssuschemeng.1c00343.

Physicochemical characterization of the catalysts: N_2 adsorption at −196 °C, transmission electron images, as well as CO-PROX catalytic activity results, XRD and H_2-TPR results from fresh and spent samples, and additional material from isotopic oxygen pulse experiments (PDF)

AUTHOR INFORMATION

Corresponding Author

Arantxa Davó-Quiñonero − *Inorganic Chemistry Department, University of Alicante, E-03080 Alicante, Spain;* orcid.org/0000-0001-9776-3458; Email: arantxa.davo@tcd.ie

Authors

Sergio López-Rodríguez − *Inorganic Chemistry Department, University of Alicante, E-03080 Alicante, Spain*

https://doi.org/10.1021/acssuschemeng.1c00343
ACS Sustainable Chem. Eng. 2021, 9, 6329−6336

Esther Bailón-García − *Inorganic Chemistry Department, University of Alicante, E-03080 Alicante, Spain;* orcid.org/0000-0001-8418-8714

Dolores Lozano-Castelló − *Inorganic Chemistry Department, University of Alicante, E-03080 Alicante, Spain*

Agustín Bueno-López − *Inorganic Chemistry Department, University of Alicante, E-03080 Alicante, Spain;* orcid.org/0000-0002-5434-6459

Complete contact information is available at: https://pubs.acs.org/10.1021/acssuschemeng.1c00343

Author Contributions

The manuscript was written through contributions of all authors. All authors have given approval to the final version of the manuscript. All authors contributed equally to this work.

Notes

The authors declare no competing financial interest.

■ ACKNOWLEDGMENTS

The authors thank the financial support of the Spanish Ministry of Economy and Competitiveness (Project CTQ2015-67597-C2-2-R and grant FJCI-2015-23769), the Spanish Ministry of Science and Innovation (PID2019-105960RB-C22), Spanish Ministry of Education (FPU14/01178), Generalitat Valenciana (Project PROMETEO/2018/076), and the EU (FEDER funding).

■ REFERENCES

(1) European Commission. Critical materials for strategic technologies and sectors in the EU-a foresight study. 2020. https://ec.europa.eu/docsroom/documents/42881 (accessed October 2020).

(2) Mancheri, N. A.; Sprecher, B.; Bailey, G.; Ge, J.; Tukker, A. Effect of Chinese Policies on Rare Earth Supply Chain Resilience. *Resour., Conserv. Recycl.* **2019**, *142*, 101−112.

(3) Wan, R.; Wen, J.-F. The Environmental Conundrum of Rare Earth Elements. *Environ. Resour. Econ.* **2017**, *67*, 157−180.

(4) Machacek, E.; Richter, J.; Lane, R. Governance and Risk−Value Constructions in Closing Loops of Rare Earth Elements in Global Value Chains. *Resources* **2017**, *6*, 59−74.

(5) Smith, B. J.; Eggert, R. G. Costs, Substitution, and Material Use: The Case of Rare Earth Magnets. *Environ. Sci. Technol.* **2018**, *52*, 3803−3811.

(6) Trovarelli, A. *Catalysis by Ceria and Related Materials*; Catalytic Science Series; Imperial College Press, 2002; Vol. *1*.

(7) Liu, B.; Zhang, Y.; Lu, M.; Su, Z.; Li, G.; Jiang, T. Extraction and Separation of Manganese and Iron from Ferruginous Manganese Ores: A Review. *Miner. Eng.* **2019**, *131*, 286−303.

(8) Dey, S.; Praveen Kumar, V. V. The Performance of Highly Active Manganese Oxide Catalysts for Ambient Conditions Carbon Monoxide Oxidation. *Curr. Res. Green Sustain. Chem.* **2020**, *3*, 100012−100027.

(9) Almquist, C.; Krekeler, M.; Jiang, L. An Investigation on the Structure and Catalytic Activity of Cryptomelane-Type Manganese Oxide Materials Prepared by Different Synthesis Routes. *Chem. Eng. J.* **2014**, *252*, 249−262.

(10) Luo, J.; Zhang, Q.; Garcia-Martinez, J.; Suib, S. L. Adsorptive and Acidic Properties, Reversible Lattice Oxygen Evolution, and Catalytic Mechanism of Cryptomelane-Type Manganese Oxides as Oxidation Catalysts. *J. Am. Chem. Soc.* **2008**, *130*, 3198−3207.

(11) Duan, N.; Suib, S. L.; O'Young, C.-L. Sol−Gel Synthesis of Cryptomelane, an Octahedral Molecular Sieve. *J. Chem. Soc., Chem. Commun.* **1995**, *13*, 1367−1368.

(12) Hernández, W. Y.; Centeno, M. A.; Romero-Sarria, F.; Ivanova, S.; Montes, M.; Odriozola, J. A. Modified Cryptomelane-Type Manganese Dioxide Nanomaterials for Preferential Oxidation of CO in the Presence of Hydrogen. *Catal. Today* **2010**, *157*, 160−165.

(13) Stelmachowski, P.; Monteverde Videla, A. H. A.; Jakubek, T.; Kotarba, A.; Specchia, S. The Effect of Fe, Co, and Ni Structural Promotion of Cryptomelane (KMn_8O_{16}) on the Catalytic Activity in Oxygen Evolution Reaction. *Electrocatalysis* **2018**, *9*, 762−769.

(14) Li, Y.; Fan, Z.; Shi, J.; Liu, Z.; Zhou, J.; Shangguan, W. Modified Manganese Oxide Octahedral Molecular Sieves M′-OMS-2 (M′=Co,Ce,Cu) as Catalysts in Post Plasma-Catalysis for Acetaldehyde Degradation. *Catal. Today* **2015**, *256*, 178−185.

(15) Hernández, W. Y.; Centeno, M. A.; Ivanova, S.; Eloy, P.; Gaigneaux, E. M.; Odriozola, J. A. Cu-Modified Cryptomelane Oxide as Active Catalyst for CO Oxidation Reactions. *Appl. Catal., B* **2012**, *123−124*, 27−35.

(16) Kumar, R.; Mittal, J.; Kushwaha, N.; Rao, B. V.; Pandey, S.; Liu, C.-P. Room Temperature Carbon Monoxide Gas Sensor Using Cu Doped OMS-2 Nanofibers. *Sens. Actuators, B* **2018**, *266*, 751−760.

(17) Dey, S.; Dhal, G. C. A Review of Synthesis, Structure and Applications in Hopcalite Catalysts for Carbon Monoxide Oxidation. *Aerosol Sci. Eng.* **2019**, *3*, 97−131.

(18) Konsolakis, M. The Role of Copper−Ceria Interactions in Catalysis Science: Recent Theoretical and Experimental Advances. *Appl. Catal., B* **2016**, *198*, 49−66.

(19) Beckers, J.; Rothenberg, G. Sustainable Selective Oxidations Using Ceria-Based Materials. *Green Chem.* **2010**, *12*, 939−948.

(20) Kašpar, J.; Di Monte, R.; Fornasiero, P.; Graziani, M.; Bradshaw, H.; Norman, C. Dependency of the Oxygen Storage Capacity in Zirconia−Ceria Solid Solutions upon Textural Properties. *Top. Catal.* **2001**, *16*, 83−87.

(21) Rico-Pérez, V.; Bueno-López, A. Effect of RhO_x/CeO_2 Calcination on Metal-Support Interaction and Catalytic Activity for N_2O Decomposition. *Appl. Sci.* **2014**, *4*, 468−481.

(22) DeGuzman, R. N.; Shen, Y.-F.; Neth, E. J.; Suib, S. L.; O'Young, C.-L.; Levine, S.; Newsam, J. M. Synthesis and Characterization of Octahedral Molecular Sieves (OMS-2) Having the Hollandite Structure. *Chem. Mater.* **1994**, *6*, 815−821.

(23) Atribak, I.; Bueno-López, a.; García-García, a.; Navarro, P.; Frías, D.; Montes, M. Catalytic Activity for Soot Combustion of Birnessite and Cryptomelane. *Appl. Catal., B* **2010**, *93*, 267−273.

(24) Lee, H. C.; Kim, D. H. Kinetics of CO and H_2 Oxidation over $CuO-CeO_2$ Catalyst in H_2 Mixtures with CO_2 and H_2O. *Catal. Today* **2008**, *132*, 109−116.

(25) Gamarra, D.; Martínez-Arias, A. Preferential Oxidation of CO in Rich H_2 over CuO/CeO_2: Operando-DRIFTS Analysis of Deactivating Effect of CO_2 and H_2O. *J. Catal.* **2009**, *263*, 189−195.

(26) Njagi, E. C.; Genuino, H. C.; King'ondu, C. K.; Chen, C.-H.; Horvath, D.; Suib, S. L. Preferential Oxidation of CO in H_2-Rich Feeds over Mesoporous Copper Manganese Oxides Synthesized by a Redox Method. *Int. J. Hydrogen Energy* **2011**, *36*, 6768−6779.

(27) Davó-Quiñonero, A.; Lozano-Castelló, D.; Bueno-López, A. Unexpected Stability of CuO/Cryptomelane Catalyst under Preferential Oxidation of CO Reaction Conditions in the Presence of CO_2 and H_2O. *Appl. Catal., B* **2017**, *217*, 459−465.

(28) Ho, P. H.; Lee, S. C.; Kim, J.; Lee, D.; Woo, H. C. Properties of a Manganese Oxide Octahedral Molecular Sieve (OMS-2) for Adsorptive Desulfurization of Fuel Gas for Fuel Cell Applications. *Fuel Process. Technol.* **2015**, *131*, 238−246.

(29) Davó-Quiñonero, A.; Navlani-García, M.; Lozano-Castelló, D.; Bueno-López, A. CuO/Cryptomelane Catalyst for Preferential Oxidation of CO in the Presence of H_2: Deactivation and Regeneration. *Catal. Sci. Technol.* **2016**, *6*, 5684−5692.

(30) Stelmachowski, P.; Legutko, P.; Jakubek, T.; Indyka, P.; Sojka, Z.; Holmlid, L.; Kotarba, A. Emission of Highly Excited Electronic States of Potassium from Cryptomelane Nanorods. *Phys. Chem. Chem. Phys.* **2015**, *17*, 26289−26294.

(31) Davó-Quiñonero, A.; Such-Basáñez, I.; Juan-Juan, J.; Lozano-Castelló, D.; Stelmachowski, P.; Grzybek, G.; Kotarba, A.; Bueno-López, A. New Insights into the Role of Active Copper Species in

CuO/Cryptomelane Catalysts for the CO-PROX Reaction. *Appl. Catal., B* **2020**, *267*, 118372−118383.
(32) Ho, P. H.; Lee, S. C.; Kim, J.; Lee, D.; Woo, H. C. Properties of a Manganese Oxide Octahedral Molecular Sieve (OMS-2) for Adsorptive Desulfurization of Fuel Gas for Fuel Cell Applications. *Fuel Process. Technol.* **2015**, *131*, 238−246.
(33) Yu, D.; Ren, Y.; Yu, X.; Fan, X.; Wang, L.; Wang, R.; Zhao, Z.; Cheng, K.; Chen, Y.; Sojka, Z.; Kotarba, A.; Wei, Y.; Liu, J. Facile Synthesis of Birnessite-Type $K_2Mn_4O_8$ and Cryptomelane-Type $K_{2-X}Mn_8O_{16}$ Catalysts and Their Excellent Catalytic Performance for Soot Combustion with High Resistance to H_2O and SO_2. *Appl. Catal., B* **2021**, *285*, 119779−119793.
(34) Vepřek, S.; Cocke, D. L.; Kehl, S.; Oswald, H. R. Mechanism of the Deactivation of Hopcalite Catalysts Studied by XPS, ISS, and Other Techniques. *J. Catal.* **1986**, *100*, 250−263.
(35) Mirzaei, A. A.; Shaterian, H. R.; Kaykhaii, M. The X-Ray Photoelectron Spectroscopy of Surface Composition of Aged Mixed Copper Manganese Oxide Catalysts. *Appl. Surf. Sci.* **2005**, *239*, 246−254.
(36) Dey, S.; Dhal, G. C. Deactivation and Regeneration of Hopcalite Catalyst for Carbon Monoxide Oxidation: A Review. *Mater. Today Chem.* **2019**, *14*, 100180−100194.
(37) Caputo, T.; Lisi, L.; Pirone, R.; Russo, G. On the Role of Redox Properties of CuO/CeO_2 Catalysts in the Preferential Oxidation of CO in H_2-Rich Gases. *Appl. Catal., A* **2008**, *348*, 42−53.
(38) Giménez-Mañogil, J.; Bueno-López, A.; García-García, A. Preparation, Characterisation and Testing of $CuO/Ce_{0.8}Zr_{0.2}O_2$ Catalysts for NO Oxidation to NO_2 and Mild Temperature Diesel Soot Combustion. *Appl. Catal., B* **2014**, *152*−*153*, 99−107.
(39) Davó-Quiñonero, A.; Bailón-García, E.; López-Rodríguez, S.; Juan-Juan, J.; Lozano-Castelló, D.; García-Melchor, M.; Herrera, F. C.; Pellegrin, E.; Escudero, C.; Bueno-López, A. Insights into the Oxygen Vacancy Filling Mechanism in CuO/CeO_2 Catalysts: A Key Step Toward High Selectivity in Preferential CO Oxidation. *ACS Catal.* **2020**, *10*, 6532−6545.
(40) Polster, C. S.; Nair, H.; Baertsch, C. D. Study of Active Sites and Mechanism Responsible for Highly Selective CO Oxidation in H_2 Rich Atmospheres on a Mixed Cu and Ce Oxide Catalyst. *J. Catal.* **2009**, *266*, 308−319.
(41) Sedmak, G.; Hočevar, S.; Levec, J. Kinetics of Selective CO Oxidation in Excess of H_2 over the Nanostructured $Cu_{0.1}Ce_{0.9}O_{2-y}$ Catalyst. *J. Catal.* **2003**, *213*, 135−150.
(42) Lykaki, M.; Pachatouridou, E.; Carabineiro, S. A. C.; Iliopoulou, E.; Andriopoulou, C.; Kallithrakas-Kontos, N.; Boghosian, S.; Konsolakis, M. Ceria Nanoparticles Shape Effects on the Structural Defects and Surface Chemistry: Implications in CO Oxidation by Cu/CeO_2 Catalysts. *Appl. Catal., B* **2018**, *230*, 18−28.

https://doi.org/10.1021/acssuschemeng.1c00343
ACS Sustainable Chem. Eng. 2021, 9, 6329−6336